Journal of Hydrology: Regional Studies 4 (2015) 550–570

Contents lists available at ScienceDirect

Journal of Hydrology: Regional Studies

journal homepage: www.elsevier.com/locate/ejrh

Estimating climate-change effects on a Mediterranean catchment under various irrigation conditions

D. von Gunten [a], T. Wöhling [a,c], C.P. Haslauer [a], D. Merchán [b], J. Causapé [b], O.A. Cirpka [a,*]

[a] University of Tübingen, Center for Applied Geoscience, Hölderlinstr. 12, 72076 Tübingen, Germany
[b] Geological Survey of Spain – IGME, C/ Manuel Lasala no. 44, 9B, Zaragoza 50006, Spain
[c] Lincoln Agritech Ltd., Ruakura Research Centre, Hamilton, New Zealand

ARTICLE INFO

Article history:
Received 25 May 2015
Received in revised form 31 July 2015
Accepted 3 August 2015
Available online 5 September 2015

Keywords:
Irrigation
Climate change
Integrated hydrological model
Mediterranean region
Hydrological response

ABSTRACT

Study region: The Lerma catchment, a small (7.3 km^2) sub-catchment of the Ebro Basin in northern Spain.
Study focus: The Lerma catchment underwent a monitored transition to irrigated agriculture, using water from outside the catchment, between 2006 and 2008. This transition has successfully been simulated using the partial-differential-equation-based model HydroGeoSphere, simulating coupled evapotranspiration, surface water, and groundwater flow in the catchment. We use the calibrated model to study how irrigation practices influence the response of the Lerma catchment to the climate change projected for northern Spain. We consider four different irrigation scenarios: no irrigation, present irrigation, climate-adapted irrigation with current crops, and adapted irrigation for crops requiring less water. The climate scenarios are based on four regional climate models and two downscaling methods.
New hydrological insight: The simulated catchment responses to climate change show clear differences between the irrigation scenarios. In future climate, groundwater levels and base flows decrease more when irrigation is present than without irrigation, because groundwater levels and base flow in present climate are already at low levels without irrigation. In contrast, annual peak discharges increase more in non-irrigated cases than in irrigated cases. Irrigation increases water availability and an associated rise in potential evapotranspiration results in higher actual evapotranspiration during summer. In non-irrigated scenarios, by contrast, actual evapotranspiration in summer is controlled by precipitation and thus decreases in future climate.

1. Introduction

The increase in mean global air temperature over the past 30 years, linked to the anthropogenic increase of CO_2 emissions (e.g., Meehl et al., 2007), influences the global and regional water cycle and is expected to change future precipitation patterns (e.g., Sillmann and Roeckner, 2008). Particularly strong impacts are expected in semi-arid regions, such as the Ebro basin in north-east Spain (Vargas-Amelin and Pindado, 2014). The timing and magnitude of these impacts, however, are difficult to

* Corresponding author.
E-mail address: olaf.cirpka@uni-tuebingen.de (O.A. Cirpka).

http://dx.doi.org/10.1016/j.ejrh.2015.08.001

predict (Ghosh and Misra, 2010), a fact which complicates efficient mitigation. In the next century, less water will probably be available in the Ebro region (Bovolo et al., 2010; Buerger et al., 2007; Milano et al., 2013) as a result of increased potential evapotranspiration (Moratiel et al., 2010; García-Garizábal et al., 2014) and decreased precipitation in spring and summer (Blenkinsop and Fowler, 2007; Ribalaygua et al., 2013).

Various catchment-scale case-studies in north-east Spain forecast a decrease in runoff (Candela et al., 2012), streamflow (Ferrer et al., 2012; López-Moreno et al., 2014; Zambrano-Bigiarini et al., 2010), recharge (Candela et al., 2012), and water quality (Bovolo et al., 2010). Some recent observed changes, for example variations in run-off generation (Otero et al., 2011) and decrease in river flow (Milano et al., 2013), have already been linked to ongoing climate change. In addition, irrigation needs are likely to increase (e.g. Jorge and Ferreres, 2001; Rey et al., 2011; Iglesias and Minguez, 1997) because of the higher evaporative demand and possibly because of expanding irrigated areas (Scanlon et al., 2007; Bielsa and Cazcarro, 2015).

Changes in land use often interact with climate change and its impacts (e.g., Dale, 1997; Pielke, 2005). For example, predictions of stream-flow in the Pyrenean mountains indicate that reforestation and climate change together lead to a decrease stream-flow twice as much as climate change alone (López-Moreno et al., 2014). In the same region, the duration of snow cover is expected to decrease due to climate change, while reforestation influences the snow depth (Szczypta et al., 2015). Reforestation also impacts climate-change effects on erosion in semi-arid regions (Simonneaux et al., 2015) and on groundwater recharge (Montenegro and Ragab, 2012). In the semi-arid Upper Yellow River region of China, land-use changes, notably over-grazing and increased irrigation, result in a decrease of stream-flow at a similar magnitude than the one due to climate change (Cuo et al., 2013; Zhao et al., 2009; Zheng et al., 2009). In general, assessing the contribution of land-use and climate changes on streamflow changes is difficult and uncertainties are large (Cuo et al., 2013; Kling et al., 2014; Mehdi et al., 2015). In irrigated regions, the choice of irrigation techniques and cropping patterns can support the adaptation to climate change (Mehta et al., 2013; Woznicki et al., 2015). However, because of water-resources limitation and increasing irrigation needs, irrigation often worsens effects of climate change on hydrological processes in semi-arid climates (e.g., Candela et al., 2009).

Because of the interactions between climate and land-use changes, the increase in irrigation needs or in irrigated area, which might be as high as 50% of the current irrigated area in the Ebro region (Bielsa and Cazcarro, 2015), is likely to have impacts beyond the direct increase in water use. Apart from its importance for the regional water resources, irrigation management might influence the response of the catchment to climate change. An irrigated and a non-irrigated catchment might react differently to the same changes in climate. However, the extent and nature of these differences in climate sensitivity is unknown.

In this study, we analyze some of these differences to better understand the interactions between irrigation and climate change. We concentrate on a catchment-scale case study, situated in north-east Spain. The Lerma catchment experienced a monitored transition to irrigated agriculture in the years 2006–2008 allowing us to simulate the hydrological processes in this catchment, before and after the implementation of irrigation. Then, we model the studied catchment assuming different irrigation scenarios and a scenario without irrigation in present and future climate. The differences in the catchment responses to climate change can be linked to irrigation practices and used to improve the understanding of interactions between climate change and irrigation. Our comparison is centered on a specific case study. However, climate, geology, and agricultural practices in many catchments in the Ebro region are similar to those in the Lerma catchment. Hence, our results are relevant for the whole region, especially because of the planned expansion of irrigated agriculture.

The remainder of this paper is structured as follows: First, we review the study area and the hydrological model. Then, we describe the climate and the irrigation scenarios. Finally, we present our results about the impact of climate change on hydraulic heads, base flows, peak flows, and actual evapotranspiration assuming different irrigation scenarios.

2. Study area

The Lerma catchment (~42.06° N, ~1.14° W, Fig. 1) is located in the central Ebro basin. Current climate is classified as semi-arid with a mean annual precipitation of 402 mm/year (2004–2011) and a mean reference evapotranspiration (ET_0) of 1301 mm/year (2004–2011) (Merchán et al., 2013). Daily precipitation and temperature have been measured since 1989 at the meteorological station of Ejea de los Caballeros, located ~5 km to the north of the catchment. Wind speed, radiation and relative humidity have been measured there since 2003. Annual total precipitation has varied between 236 mm/year and 630 mm/year over that period of time. Most rains fall in autumn and spring, while summers are usually drier and characterized by long periods of anticyclonic conditions.

The catchment is about 7.3 km^2 large with elevation ranging between 330 meters above sea level (masl.) and 490 masl. Agriculture is currently the dominant land use (Pérez et al., 2011). However, prior to 2006, irrigated agriculture was not practiced in the catchment. Irrigation started in April 2006 and has been expanding since. Currently, the area of irrigated land is about half of the watershed. The volume of irrigation was 2.1×10^6 m^3/year in 2011 (Merchán et al., 2013) and none prior to 2006 (Table 1). Irrigation is recorded daily in 52 zones, which are generally defined based on the limits of the fields owned by each farmer. The majority of irrigation is applied from April to September and the main cultivated crops are corn, winter cereal, and sunflower (Table 2). The irrigation water is provided from the Aragon river whose flow is stored in the Yesa reservoir, situated about 70 km to the north of the catchment in the Pyrenees. After being transported using the Bardenas irrigation canal, the irrigation water is distributed in the catchment using sprinklers in 86% of the irrigated area and drip irrigation otherwise (Abrahao et al., 2011). No groundwater is used for irrigation or for water supply within the catchment.

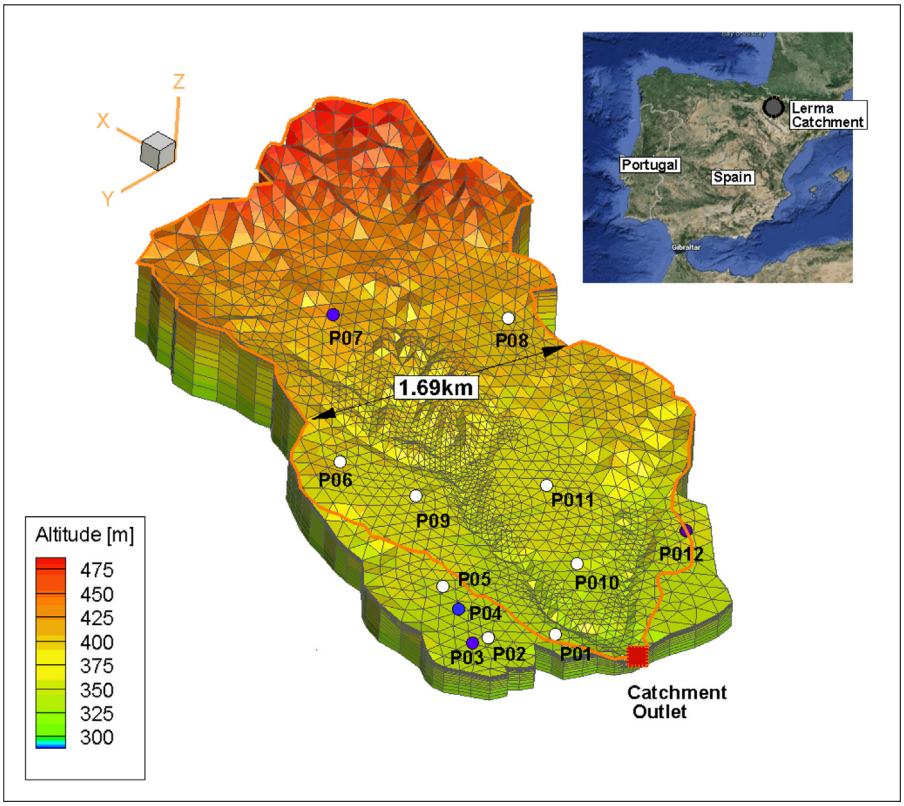

Fig. 1. Elevation of the Lerma catchment (masl.) and the computational grid of the hydrological model. Vertical exaggeration: 5:1. The catchment outlet is indicated by a red square, the wells installed in 2008 are indicated by white dots, and the ones installed in 2010 by blue dots. The orange line represents the limits of the surface-flow domain. (For interpretation of the references to color in this figure legend, the reader is referred to the web version of the article.)

Table 1
Yearly volume of irrigation – from Merchán et al. (2013).

Year	Irrigation [hm^3]
2005	0.00
2006	0.62
2007	1.59
2008	2.00
2009	2.01
2010	2.03
2011	2.07

Table 2
Area of cultivated crops in the Lerma catchment for 2009–2011, in % of total irrigated area (3.54 km^2). Year 1, 2, and 3 are used to define the 4th irrigation scenario. (Section 5).

Crop type	Present			Future		
	2009	2010	2011	Year 1	Year 2	Year 3
Corn	39	36	47	15	13	20
Winter cereal	15	18	12	39	40	38
Tomato	8	5	0	8	5	0
Sunflower	13	3	8	0	0	0
Grass	4	3	4	17	6	12
Other crops	5	26	23	5	27	24
Fallow	16	9	6	16	9	6

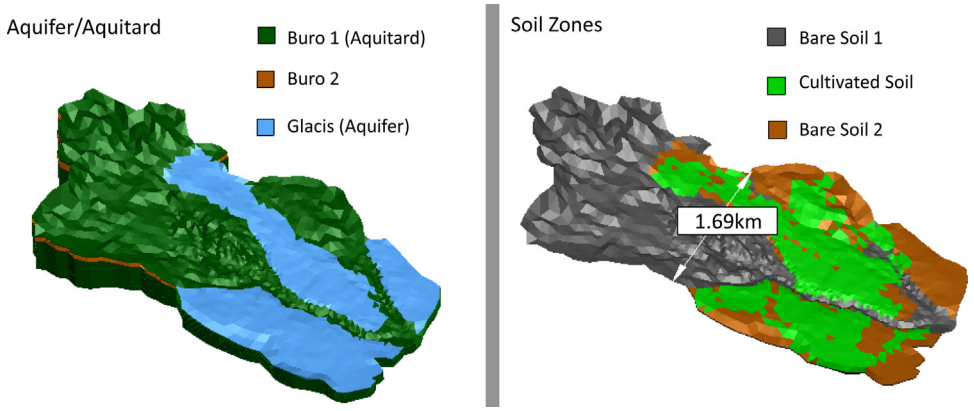

Fig. 2. Conceptual model of the catchment: hydrogeological and soil units. Vertical exaggeration: 5:1. Extent of the cultivated soil is shown for the year 2009, present cropping pattern. Modified from von Gunten et al. (2014).

The subsurface of the catchment can be conceptualized as an unconfined aquifer lying above an aquitard. The aquifer, denoted glacis, is composed of permeable, clastic, and unconsolidated deposits from the Quaternary period. It covers about half of the surface of the catchment, in the regions where agriculture is the most intensive. The thickness of this aquifer (average thickness: 6.5 m, maximum thickness:12.6 m) was measured at 12 observation wells and estimated at 63 other locations during an electrical sounding survey (Plata-Torres, 2012). The aquitard, denoted buro, is a Tertiary bedrock made of lutite and mudstones. The soil layer is shallow, 0.3-0.9 m deep (Beltrán, 1986), and composed of inceptisols (Pérez et al., 2011).

Many studies have been conducted in the Lerma catchment to explore the impacts on the catchment of the transition to irrigated agriculture (Abrahao et al., 2011; Merchán et al., 2013, 2014; Pérez et al., 2011; Skhiri and Dechimi, 2011; Urdanoz and Aragüés, 2011), and measurements are ongoing. Hydraulic heads in the glacis have been measured since March 2008 in eight wells, usually with a monthly frequency. In 2010, four additional observation wells were drilled (Fig. 1). Stream flow discharge at the catchment outlet has been measured since 2006 with a temporal resolution of 15 min. Crop types for each agricultural plot are recorded and planting dates for the region of Ejea de los Caballeros are obtained from Martínez-Cob (2004). A digital elevation model with a horizontal resolution of 5 m (IGN, 2012) was used.

3. Hydrological model

The model used in the study and its calibration have previously been described by von Gunten et al. (2014). Therefore, only a brief summary is given here.

3.1. Conceptual model

The subsurface of the Lerma catchment is separated into six zones, based on the local geology (Fig. 2). The deepest zone represents the buro (aquitard). The aquifer, denoted glacis, forms the second zone. In the parts of the domain where the buro is close to the ground surface, a thin layer exists that represents a weathered zone of the buro with an increased hydraulic conductivity. The soil layer is divided into three zones: the first represents the bare soil above the glacis, the second the bare soil above the buro, and the third the cultivated soil. All zones are considered internally homogeneous and anisotropic with the horizontal permeability being ten times larger than the vertical one.

The surface domain is separated into 55 zones representing fields of different crops (Table 2), described by a seasonal leaf area index and a constant root depth (as given by Pérez et al., 2011; von Gunten et al., 2014). These fields are very similar to the 52 zones used for irrigation inputs (Section 2). The difference between surface and irrigation zones is that three irrigation zones are separated in two halves each, representing areas with different crops. Manning's roughness coefficient n, and thus surface run-off, depends on the crop type and hence is assigned depending on the above described zones. Daily crop evapotranspiration under standard conditions (ET_c), corresponding to the maximum evapotranspiration of each crop without water limitation, is calculated using the FAO version of the Penman-Monteith equation (Allen et al., 2000). The spatial variability of the crops on the field scale is taken into account by multiplying the reference evapotranspiration by a time-varying crop coefficient. We use different crop coefficients, directly taken from Allen et al. (2000), for the 10 main crop types cultivated in the catchment. Precipitation inputs are described by daily values for mild precipitation events (less than 25 mm/day). During more intense precipitation events, the total daily precipitation is assumed to occur within 3 h during summer and spring, and within 9 h during autumn and winter. This procedure mimics intense convective precipitation events that frequently occur in this area, especially during summer (von Gunten et al., 2014).

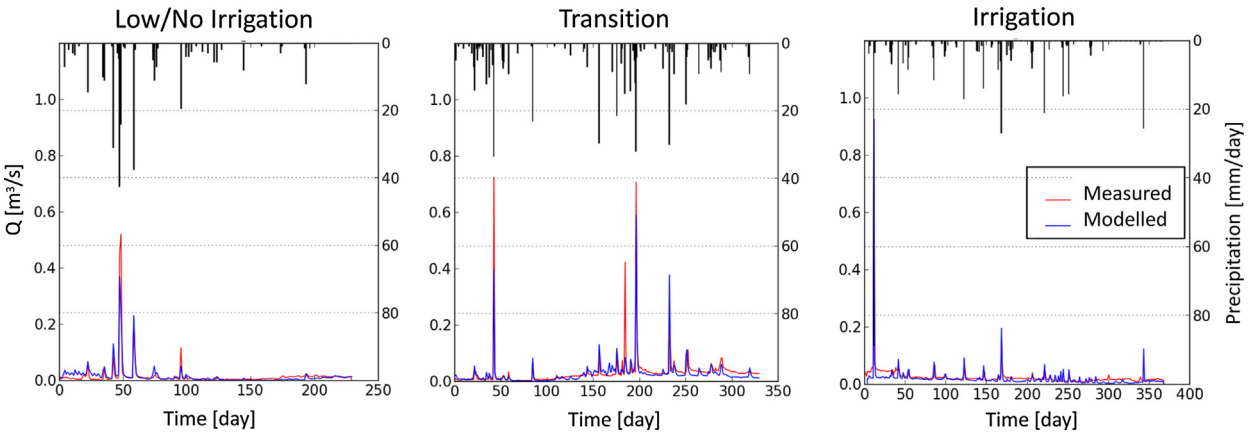

Fig. 3. Measured and modeled hydrograph for a period with no irrigation (start: 15th March 2007, left panel), a transition period (start: 18th May 2008, middle panel), and a period with large irrigation (start: 26th Oct. 2010, right panel). Modified from von Gunten et al. (2014).

A no-flow boundary condition is assumed at the bottom and the lateral sides of the sub-surface model domain. The boundaries of the model domain are based on the boundaries of the aquifer in the lower part of the catchment and on the surface catchment in the upper part of the domain, where there is no permeable layer (glacis). The boundaries of the aquifer are derived from an electrical sounding campaign (Plata-Torres, 2012) and the boundaries of the surface catchment are based on topography. The surface catchment is slightly smaller than the model domain. Hence, surface runoff outside the surface catchment is allowed to leave the model domain by assuming a critical-flow-depth boundary condition at the lateral boundaries of the domain. The computational grid is composed of ~80,000 elements separated in 22 horizontal layers. The mean surface area of the elements is about 0.2 ha and the thickness of the computational layers varies between 8 mm and 25 m, but is about 1–3 cm for the three first layers.

3.2. Numerical model

The hydrological model used in this study, HydroGeoSphere (Therrien, 2006; Therrien et al., 2010), is a well-established spatially distributed partial-differential-equation-based model. This type of model was more suitable than simpler conceptual models to simulate the hydrological changes due to the onset of irrigation (Pérez et al., 2011). In addition, the impacts of climate change on surface and subsurface water bodies can jointly be studied. Moreover, the coupling between surface and subsurface, and the low reliance of this kind of model on empirical relationships might improve its predictive power (Goderniaux et al., 2009).

In HydroGeoSphere, variably-saturated subsurface water flow is modeled using the three-dimensional Richards' equation (Richards, 1931). To solve the Richards' equation, a constitutive relationship between water saturation, relative permeability, and hydraulic heads is needed. In this study, we use the well-known Mualem-van-Genuchten parametrization (van Genuchten, 1980). The surface flow is simulated using the diffusive-wave approximation of the two-dimensional Saint Venant equations (Moussa and Bocquillon, 2000). The calculation of actual evapotranspiration depends on ET_c, soil–water saturation, and crop types (Therrien et al., 2010). Surface and subsurface flow are coupled by the dual-node approach (Therrien et al., 2010). Infiltration and exfiltration are conceptualized using an approach adapted from Darcy's law. The flow between the surface and the subsurface domains is a function of the head differences between the two domains, the relative permeability, and the coupling length, which is a parameter describing the connectivity between the surface and the subsurface. Irrigation and precipitation are implemented as a prescribed volume flux per area to each element. Precipitation is applied to the whole model domain, while irrigation is assigned to the area of each individual field.

3.3. Model calibration

von Gunten et al. (2014) presented the calibration of the model using a hierarchy of grids. Hydraulic heads in 12 observations wells and the hydrograph at the catchment outlet for the years 2006–2009 were used to calibrate the model parameters which had been identified as the most sensitive ones with respect to the calibration targets (i.e., the hydraulic conductivity in all model zones, except from the zone representing the weathered buro, the porosity, and the van-Genuchten parameters in the soil zones). Model validation was performed using the same data types for the years 2010–2011. More details on the calibration have been reported by von Gunten et al. (2014) and are not repeated here. The result of the calibration for the hydrograph and the observation wells are reproduced in Figs. 3 and 4. The Nash-Sutcliffe efficiency (NSE, Nash and Sutcliffe, 1970) is larger than 0.7 for discharge (Table 3), and the difference between measured and modelled mean hydraulic heads is less than 2 m, which is close to the annual variability in most wells. Moreover, the variability of the hydraulic heads is

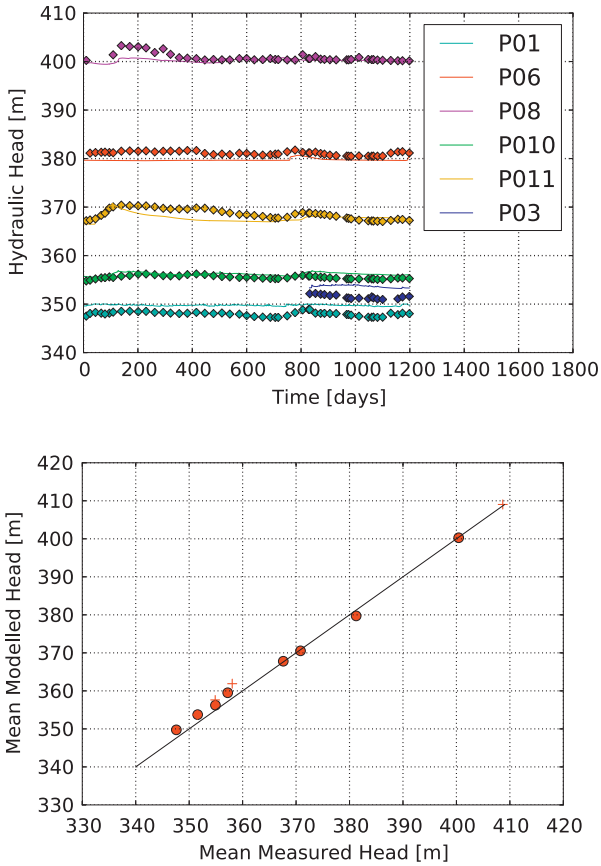

Fig. 4. Left panel: Measured (squares) and modeled (solid lines) transient hydraulic head for selected wells (start: 1st October 2008). Right panel: Average modeled and measured hydraulic-head values for all wells (2008–2011). The wells are from the lowest to the highest hydraulic head: PO1, PO2, PO3, PO10, PO4, PO5, PO12, PO11, PO9, PO6, PO8, PO7. Modified from von Gunten et al. (2014).

Table 3
Goodness-of-fit measures for calibration and validation periods. Spring of 2010 is excluded from the analysis because of strong snow events and because of the breakage of the main irrigation pipe, causing a flooding in the study area. From von Gunten et al. (2014).

	2006–2009	2010–2011
NSE	0.74	0.92
RMSE [%]	3.16	1.36

Table 4
Calibrated parameters for hydraulic conductivity, porosity and van Genuchten parameters. From von Gunten et al. (2014).

Parameter	Units	Calibrated value	Parameter role
K_{bs1}	m/s	$3*10^{-6}$	Hydraulic conductivity – Bare soil 1
K_{bs2}	m/s	10^{-6}	Hydraulic conductivity – Bare soil 2
K_{cs}	m/s	$8*10^{-5}$	Hydraulic conductivity – Cultivated soil
K_{g1}	m/s	$1.7*10^{-4}$	Hydraulic conductivity – Glacis
K_b	m/s	10^{-7}	Hydraulic conductivity – buro
α_{bs1}	1/m	4.95	van Genuchten parameter – Bare soil 1
α_{bs2}	1/m	4	van Genuchten parameter – Bare soil 2
α_{cs}	1/m	4	van Genuchten parameter – Cultivated soil
n_{bs1}	–	1.35	van Genuchten parameter – Bare soil 1
n_{bs2}	–	1.4	van Genuchten parameter – Bare soil 2
n_{cs}	–	1.35	van Genuchten parameter – Cultivated soil
$\theta_{s,g1}$	–	0.2	Porosity – Glacis

Table 5
Name and acronym of the analyzed regional climate model from the ENSEMBLES project. Adapted from (Herrera et al., 2010).

Acronym	RCM	GCM	References
ETHZ	CLM	HadCM3	Jaeger et al. (2008)
METO	HadRM3	HadCM3	Collins et al. (2006)
MPI	M- REMO	ECHAM5	Jacob et al. (2001)
UCLM	PROMES	HadCM3	Sánchez et al. (2004)
METNO	HIRHAM	HadCM3	Haugen and Haakensatd (2005)
KNMI	RACMO	ECHAM5	van Meijgaard (2008)
CNRM	ALADIN-Climat	ARPEGE	Radu et al. (2008)
ICTP	RegCM3	ECHAM5	Pal et al. (2007)
SMHI	RCA	ECHAM5	Kjellström et al. (2005)
DMI	HIRHAM	ARPEGE	Christensen et al. (2006)

generally reproduced by the model, even if annual variability is sometimes underestimated in the wells close to the aquifer boundary (such as PO1, PO8 or PO9). Calibrated parameters are presented in Table 4.

4. Climate scenarios

In this study, future CO_2 emissions follow the IPCC scenario A1B (Nakićenović et al., 2000), which consists of a generally large CO_2 flux and rapid economic growth, consistent with an increase in irrigated agriculture. Climate predictions resulting from this emission scenario are based on the ENSEMBLES project (Hewitt and Griggs, 2004 http://www.ensembles-eu.org), which proposed future climate scenarios for Europa, based on ten regional climate models (RCM) driven by three global climate models (GCM). Table 5 lists the different RCMs and GCMs used in this study.

4.1. Choice of regional climate model

Because the various climate models are constructed differently, notably in the representation of cloud physics (van der Linden and Mitchell, 2009) and of land surface/atmosphere interactions (Flato et al., 2013), a relatively large inter-model variability can be observed in the ENSEMBLES forecast (van der Linden and Mitchell, 2009). For example, predicted changes in mean winter precipitation for 2050 on the Iberian Peninsula vary between −30% and +20% of the present precipitation (van der Linden and Mitchell, 2009). Estimation of future climate impacts is therefore usually based on the output of more than one combination of regional and global climate models (Tebaldi and Knutti, 2007). Nevertheless, incorporating the outputs from regional climate models that poorly reproduce the measured local meteorological variables during the control simulation most likely deteriorates the quality of the prediction (Herrera et al., 2010). Therefore, in order to create meaningful climate scenarios, it is necessary to choose the more suitable regional climate models. While precipitation is especially important for hydrological catchment responses, it is difficult to predict (Ghosh and Misra, 2010). The reproduction of local and regional precipitation is therefore used in this study to select regional climate models for future climate predictions. This analysis is based on the assumption, commonly applied in environmental modeling, that reproducing the observed time series is a pre-requisite to predict future conditions (e.g., Hill and Tiedeman, 2007). However, reproducing the observations alone does not insure an adequate prediction, which depends on the skill of the model to reproduce changes, such as an increase in temperature. Regional and global climate models are, however, generally based on conservation principles, which hold in all climates. Moreover, they have been validated by testing their ability to reproduce climate change of the past, such as cooling caused by historical volcano eruptions (Yokohata et al., 2005) or the last glacial maximum (Kubatzki et al., 2006). Hence, we assume that the selected regional climate models will predict the future climate adequately.

To perform the model selection, we compare the precipitation output of the control simulation of the 10 regional climate models listed in Table 5 and the measured precipitation at the station of Ejea de los Caballeros. The RCM cell containing the Lerma catchment and the mean of the 8 cells of the RCM surrounding the study area were considered to rank the performance of each regional climate model. We compared monthly mean and standard deviation of the precipitation, the number of dry days in each month, and the root mean square error between the frequency distributions of modeled and measured daily precipitation. For each tested statistic, a rank was given to each model and all the ranks were added to find the most suitable models (Table 6). Four RCMs (ETHZ, METO, MPI, and UCLM) outperform the other regional climate models, based on the considered statistics.

Because of the small number of computational cells involved, the comparison described above can be misleading. Measurements and RCM outputs might be similar at a local level even though they do not reproduce the regional climate well. Consequently, we checked our results using a study of Herrera et al. (2010) who compared measured precipitation and output from the ENSEMBLES project across Spain. In this study, five regional climate models (MPI, ETHZ, UCLM, METO, and KNMI) are found to have a noticeably higher spatial correlation (between 0.7 and 0.8) with the measurements than the four other (The ICTP model was not considered by Herrera et al. (2010)). Because their ability to reproduce the local and regional precipitation, we use the MPI, ETHZ, UCLM, and METO regional climate models to create climate scenarios for the Lerma catchment.

Table 6
Ranks of the RCM for the reproduction of mean monthly precipitation (Mean), monthly standard deviation (Std), frequency distribution (Freq), number of dry days (Dry) in the Lerma catchment and the spatial correlation between the Spanish yearly climatology and the different RCMs from Herrera et al. (2010) (Corr). The ranks ranges from 1 (best) to 10 (worst). Hence, the better models have the smaller marks. The models selected for the production of the climate scenarios are indicated in bold fonts. Days are considered dry if less than 1 mm/day of precipitation is recorded.

RCM	Mean	Std	Freq	Dry	Corr	Total
ETHZ	2	2	2	2	3	11
METO	1	5	1	1	5	13
MPI	3	1	3	5	4	16
UCLM	6	4	5	3	2	20
METNO	5	7	4	4	6	26
KNMI	7	8	7	6	1	29
CNRM	4	3	6	7	9	29
ICTP	9	9	10	10	–	(38)
SHMI	8	6	8	9	8	39
DMI	10	10	9	8	7	44

4.2. Downscaling of the climate scenarios

Because of the mismatch between the scale of the outputs of the RCM (625 km^2) and of the study area (7.3 km^2) and because of the modeling uncertainties related to the climate models, RCM outputs cannot directly be used as input for the hydrological simulations (van Roosmalen et al., 2011). Instead, it is necessary to downscale the raw climate scenarios to the catchment scale. There are different methods to downscale climate inputs (Wilby and Wigley, 1997) which may result in significantly different scenarios. While no downscaling method has been univocally identified as superior over all others (Fowler et al., 2007), stochastic methods based on weather generators are often considered advantageous (Goderniaux et al., 2011; Holman et al., 2009) as they consider natural climate variability. We have used this approach as the main method to downscale the outputs of the regional climate models. To test the consistency of our results, we additionally used a quantile-based bias-correction method. Both downscaling methods are briefly presented here.

4.2.1. Downscaling by a weather generator

A weather generator is a statistical model that generates artificial time series of meteorological variables with a set of defined statistical properties that are identical to those of a reference time series. In this study, we use the RainSim weather generator (Burton et al., 2008) for precipitation and the EARWIG weather generator (Kilsby et al., 2007) for temperature, radiation, relative humidity and ET_0. RainSim is based on a Neyman-Scott rectangular pulses stochastic model (Burton et al., 2008) while EARWIG is based on first-order autoregressive processes, separating dry and wet periods (Kilsby et al., 2007). Both weather generators have been used for downscaling purposes before (e.g. Burton et al., 2010; Goderniaux et al., 2011).

The weather generators are calibrated using 24 years of daily precipitation (1989–2012) and 8 years of daily radiation, relative humidity, maximum, and minimum temperature (2004–2012) from the station of Ejea de los Caballeros. After the calibration, the RainSim performance has been evaluated by the following statistical properties of precipitation: Monthly mean, monthly variance, number of dry days, monthly skewness, frequency distribution of dry spells, frequency distribution of wet spells, annual daily maximum, and the length of longest period of the year without precipitation. Afterwards, the performance of EARWIG has been evaluated by the monthly mean of minimum and maximum daily temperature, sunshine hours, and relative humidity as well as the mean and the variance of the reference evapotranspiration. Fig. 5 presents the results of the weather-generator evaluation for the mean and skewness of precipitation, the mean, and variance of evapotranspiration and the length of dry spells. The other tested variables are not shown here for brevity, but results are similar. For each variable, the difference between the modeled and measured yearly average is less than 8%, except for the difference in the mean ET_0 variance which is 10.6%. The variables which are not directly used to calibrate the weather generators, such as the skewness of the precipitation or the frequency of dry spells, perform similarly (less than 8% of difference) as the calibrated ones.

To downscale future precipitation using RainSim, monthly change factors are extracted from the regional climate models, following the approach of Burton et al. (2010). Monthly mean rainfall, duration of dry spells, mean monthly variance and 1-day auto-correlation from the 1990 to 2000 decade are compared to the 2040–2050 decade in each regional climate model. Statistical properties of the calibrated weather generators are corrected using these change factors to calibrate RainSim for the future climate. For ET_0, a similar procedure is carried out in EARWIG. In this case, we use the mean monthly temperature, the variance of daily temperature, the mean and variance of the daily temperature range, the monthly mean of relative humidity, and the sunshine hours as target properties. We use 30 realizations of the weather generators, i.e., 30 modeled time series of daily precipitation and ET_c with a duration of 8 years each, for each group of hydrological simulations. The number of realizations was chosen by running the hydrological model with 100 realizations of the present climate without irrigation. We compared hydraulic heads in four observations wells (PO8, PO9, PO10, PO11), actual evapotranspiration (AET), and the yearly maximum and mean discharge at the outlet. The average value and variance of these hydrological variables over all realizations is very similar when more than 20 simulations were considered. We use 30 realizations, a number that was also considered to be sufficient in a case study in Belgium (Goderniaux et al., 2011).

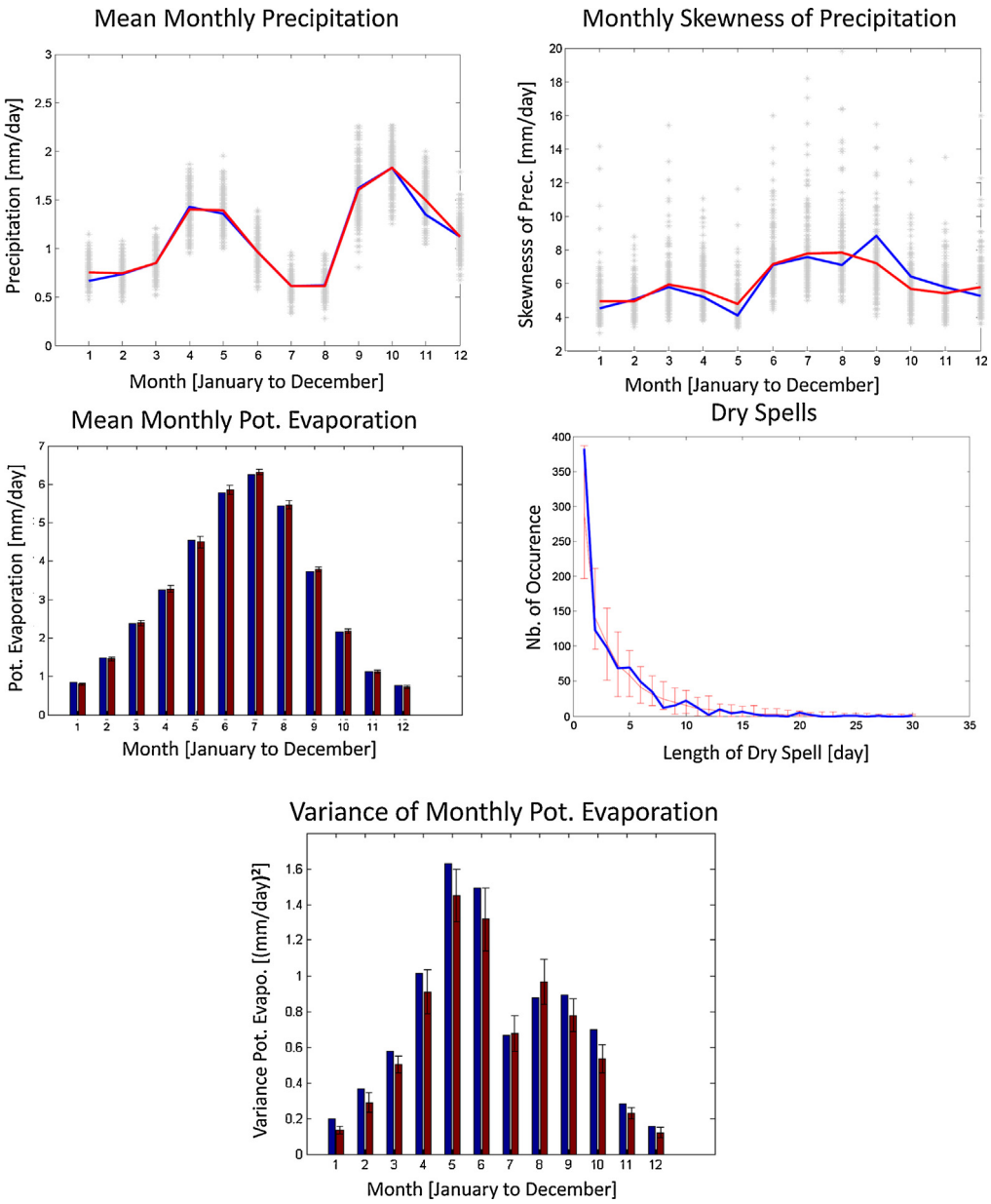

Fig. 5. Validation of the weather generator: mean and skewness of precipitation, length of dry spell, and mean and variance of reference evapotranspiration. The measured data are shown in blue and the model results in red. The error bar (bottom figures) and the gray stars (top figure) are showing the spread of the different realizations of the weather generator. (For interpretation of the references to color in this figure legend, the reader is referred to the web version of the article.)

4.2.2. Bias correction based on the mapping of quantiles

The quantile-map approach, summarized in Eq. (1), is a downscaling method which compares the frequency distribution of measured and modeled meteorological variables (Li et al., 2009). It is assumed that the computed differences are stable over time. Practically, for each value x_i of a meteorological variable for the future climate, the corresponding percentile of this variable is found in the modeled simulation for the present climate, given by the frequency distribution F_{crtl}. The bias corrected value x_{corr} of this variable for the future climate is then found in the inverse of the frequency distribution of the measured data F_{mes}.

$$x_{corr} = F_{mes}^{-1}(F_{crtl}(x_i)) \tag{1}$$

Using this method, the RCM output in a future climate can be corrected to create future climate scenarios, which are consistent with measurements and predictions from the regional climate models. We use outputs of the regional climate models from 1990 to 2000 to compare the measured and modeled frequency distribution of daily precipitation, minimum

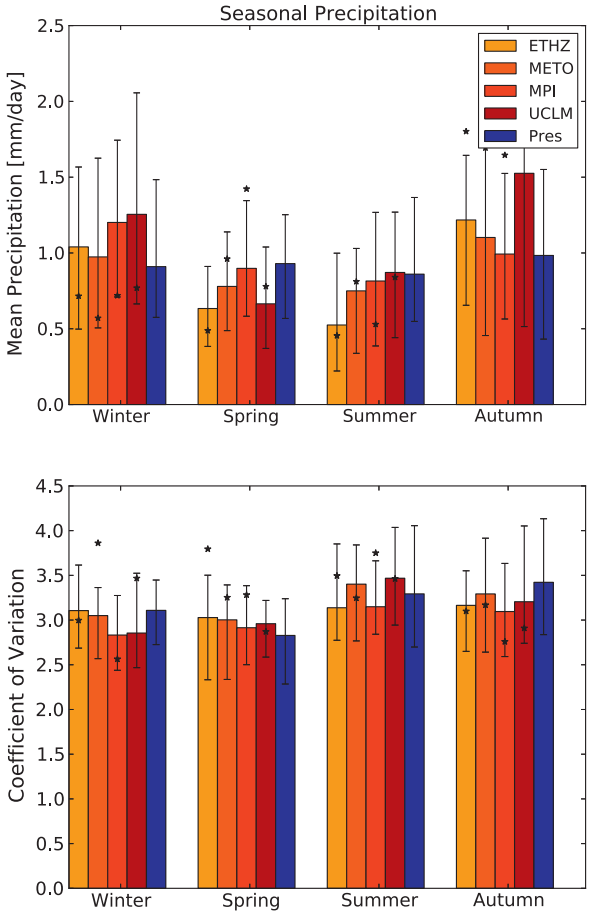

Fig. 6. Monthly mean and coefficient of variation for present and future precipitations. Based on IPCC A1B emission scenarios for 2040–2050. The error bars represent the span of the 30 realizations of the weather generator. The scenarios that are downscaled using the quantile–quantile transformation are indicated by stars. Meteorological seasons are used.

and maximum daily temperature, relative humidity, and short-wave radiation. This method produces daily time series, but the frequency distribution is based on monthly data to better reproduce the temporal auto-correlation (e.g., Ntegeka et al., 2014). The RCM outputs for the years 2040–2050 are used to create the scenarios for future climate.

4.3. Results from the climate projections

4.3.1. Precipitation

The RCM predictions for changes in mean annual precipitation differ among each other. The MPI and UCLM models forecast an increase in precipitation while the two other RCMs (ETHZ and METO) forecast a decrease. We aggregated the average predicted precipitation and the variance by season (Fig. 6) for comparison purposes. All regional climate models predict an increase in precipitation in winter and autumn (between 1% and 55%) and most models predict a decrease in summer and spring precipitation (between 3% and 39%). UCLM predicts a small precipitation increase (1.3%) during summer, which is probably not significant. Blenkinsop and Fowler (2007) found a similar seasonal pattern for the Ebro region, using regional climate models from the PRUDENCE project (Christensen and Christensen, 2007) for 2070–2100 and the A2 emission scenarios (Nakićenović et al., 2000).

Considering precipitation variability, the coefficient of variation decreases in autumn and winter (between −0.1 and −10%) and increases in spring (between +3 and +6%). Results are not unequivocal for summer (between −5% and +5%). Overall, the precipitation results from the quantile-mapped downscaling method are in agreement with those from the weather generator, i.e., the results from the quantile-mapped method fall into the spread of the realizations of the weather generator.

4.3.2. Reference evapotranspiration

Reference evapotranspiration (ET_0) increases in all RCM predictions (Fig. 7) because of the predicted increase in temperature and because of the predicted changes in relative humidity and solar radiation. The increase in total annual ET_0 ranges

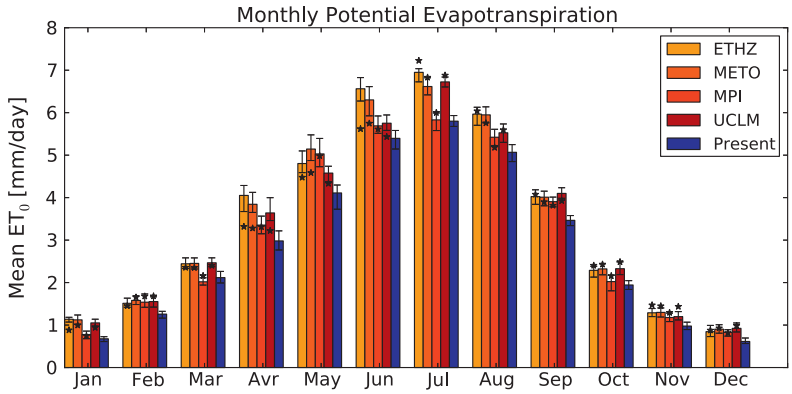

Fig. 7. Comparison of present and future ET_0. IPCC A1B emission scenarios for 2040–2050. The error bars represent the span of the 30 realizations of the weather generator. The scenarios downscaled using the quantile mapped method are indicated by stars.

from 9% in UCLM to 22% in ETHZ, and is higher in summer than in winter. A small decrease in the coefficient of variation of ET_0 is predicted, for example, from 0.3 under current conditions to 0.28 under future conditions in the ETHZ case. Variations between the realizations of the weather generator for ET_0 are low, compared to the differences between the realizations of the weather generator for precipitation.

The climate scenarios for ET_0 downscaled with the quantile mapped methods are in general similar to those using the weather generator (Fig. 7). However, ET_0 predictions based on the weather generator for ETHZ and METO between April and June are larger than the results based on the quantile-mapped method, i.e., the results from the quantile-mapped method fall under the spread of the realizations of the weather generator in these cases.

4.4. Length of observation time series and hydrological simulations

Climate change should not be confused with weather variability. Long time series are therefore necessary to create stable averages, which do not depend on short-term weather variations. This is especially important when considering precipitation. In our case, precipitation has been measured for 24 years, which was found to be sufficient to validate the weather generator. Shorter precipitation measurement time series have been used successfully in other climate-impact studies (e.g., Bouraoui et al., 1999; Fujihara et al., 2008). The time series of relative humidity, temperature, and short-wave radiation used in the present study have a duration of 8 years only, but these variables exhibit a lower variability. Therefore, we assume that the computed averages are meaningful. It is further assumed that the weather generator reproduces the general characteristics of the measured ET_0 time series (Section 4.2.1 and Fig. 5), even if the measured time series are relatively short.

We chose a length of 8 years for each of the 30 hydrological simulations (Section 4.2.1). We did not model the 240 years consecutively to reduce simulation time. In each hydrological simulation, the first two years were found to be sufficient to let the model equilibrate to the new climatic conditions ("spin-up"). These years are not considered in the analysis. While surface water reacts quickly, usually in less than a day, groundwater responds more slowly, but the aquifer is shallow (maximum depth: 12.6 m) and has a relatively large hydraulic conductivity, with a calibrated value of 1.7×10^{-4} m/s, consistent with local observations (Pérez, 2011). In addition, we found similar results for the cumulated distribution function of discharge and hydraulic head in observation wells for the scenarios without irrigation and with present irrigation when we used three or four years as spin-up periods. Consequently, we produced 30 realizations with a duration of 8 years each with the weather generator. The total length of the simulated time series is therefore $(8-2)$ years $\times 30 = 180$ years for each climate and irrigation scenario. The results using meteorological forcings that were downscaled with the quantile mapped method are used to validate the simulations whose forcings were based on the weather generators.

5. Irrigation scenarios

5.1. Methodology

To compare the impact of climate change under different agricultural managements, we considered four irrigation scenarios, representing potential agricultural practices. These scenarios were combined with the climate predictions presented above.

1. No irrigation: In this scenario, the catchment is not used for agriculture. This reflects the situation in the Lerma catchment in the years 2003–2005 and in many catchments in the Ebro region. Currently, only about 11% of the Ebro region is irrigated (Milano et al., 2013).

2. Present irrigation: Observed irrigation and crop types of the years 2009, 2010, and 2011 (Table 2) are used in the following order: 2009, 2010, 2009, 2010, 2011, 2009, 2010, 2011, with the two first years used for model spin-up. Daily distribution of irrigation at field scale is identical to the measured one.
3. Future irrigation and present cropping pattern: We use the same crop types as in scenario 2, but the irrigation volume is increased to adapt to the higher evaporative demand. Future irrigation I_{fut} [mm/day] is calculated using the following estimate (Towes and Allen, 2009):

$$I_{fut} = R_I \cdot ET_c - P_{eff} \tag{2}$$

in which ET_c is the daily crop evapotranspiration under standard condition during the irrigation season [mm/day] and P_{eff} the seasonal effective precipitation [mm/day], which is the infiltrating portion of precipitation, estimated as all precipitation under 25 mm/day, based on the definition of mild precipitation in Section 3.1. The excess precipitation (>25 mm/day) is assumed not to contribute to crop growth. R_I [-] represents the effectiveness of irrigation, which is assumed to be identical to the present one. It is calculated to be 1.06, based on data from 2009, 2010, and 2011. Values of $R_I > 1$ indicate that irrigation is larger than ET_c. However, because of surface run-off, infiltration, and soil salinisation risks due to poor irrigation practices, this value is small and shows, on average over the catchment, a well-managed irrigation or even a deficit in the total irrigation. For comparison, Towes and Allen (2009) obtained an R_I between 1.2 and 2.2 in a case study in the Okanagan basin in Canada. A similar observation about irrigation volume has been made by Abrahao et al. (2011) who note that the agricultural production did not reach the maximum potential of the area, possibly because of a water deficit.

Daily distribution of irrigation is identical in our hydrological simulation under present and future climate to reflect the local irrigation management. Under current irrigation management practices, the farmers have to order irrigation water some days before it is available. In addition, there is no precipitation in about 90% of the days in present and future climate during the irrigation period. Therefore, the amount of irrigation water is only weakly linked with daily precipitation and daily precipitation cannot be used to determine the temporal distribution of future irrigation. The spatial and temporal distribution of measured irrigation is used as model input in future climate to reflect growth distribution, crop growth, and irrigation variability between the farms. However, the total amount of irrigation depends on seasonal precipitation, a behavior reproduced by Eq. (2).

4. Future cropping pattern: Predicting the response of the farmers to climatic changes is difficult as their decision is influenced by uncertain social and economic factors in addition to climatic conditions. Their future choice of cropping patterns/crops is therefore unknown. However, we can use their response to recent weather variability as an estimate for future cropping patterns. García-Garizábal and Causapé (2010) record crop types in 2000 and 2007 in the Bardenas Canal Irrigation District no.V, a catchment close to the Lerma catchment with a similar geology and climate. In 2000, water in the Yesa reservoir, which supplies both this irrigation district and the Lerma catchment, was sufficient to meet the irrigation demand. However, in 2007, the water in the reservoir was low and usage had to be restricted. The farmers responded by decreasing the area of their corn fields by about 50% and of their sunflower fields by 90%. Instead, they increased the proportion of winter cereal and grass by 50%. Based on these observations, we assume the following changes in our scenarios with the cropping patterns:
   - Sunflowers fields are replaced by grass fields.
   - Half of the corn fields are replaced by fields of winter cereal. The modified fields are selected so that about half of the area planted with corn is covered by winter cereal.

   These changes are summarized in Table 2. The created cropping patterns were used in the following order: Year 1, Year 2, Year 1, Year 2, Year 3, Year 1, Year 2, Year 3 (Table 2), with the two first years used for model spin-up.

In our analysis, we did not consider any change in plant physiology or plant reaction to increased CO_2 availability. Planting dates are assumed to be identical in present and future climate. These dates are actually influenced by climate but determined by the farmer's management choices. Consequently, a determination of the planting dates based only on temperature changes (as by Serrat-Capdevila et al., 2011) would be inconsistent with actual management practices. We did not consider any change in the length of the growing season.

In all our hydrological simulations, we use the same model parameters as described by von Gunten et al. (2014) (Table 4). When parameters depend on the crop type, as it is the case for Manning's n, the leaf area index, and the rooting depth, they are updated to be consistent with the irrigation scenario. No cultivated zone (indicated in light green in Fig. 2) is present in Scenario 1, in which agriculture is absent.

5.2. Projected irrigation demand

Based on Eq. (2), we predict an increase in irrigation demand of 9.2% on average under future climatic conditions with the present-day cropping pattern. Our results are consistent with earlier studies for the Ebro region (Table 7). Three studies out of five (Fischer et al., 2007; Rey et al., 2011; Jorge and Ferreres, 2001) predict an increase in irrigation demand between 6% and 11%. Two other studies (Döll, 2002; Iglesias and Minguez, 1997) indicate a larger range (3–20%) of future irrigation

Table 7
Predicted irrigation changes in the Ebro region and comparison with literature.

Study	Crops	Model[a]	CO_2-related plant change	Emission scenario[b]	Irrigation increase
This study – ETHZ	Various	ET_c – P	No	A1B/2050	10.3%
This study – METO	Various	ET_c – P	No	A1B/2050	10.6%
This study – MPI	Various	ET_c – P	No	A1B/2050	6.6%
This study – UCLM	Various	ET_c – P	No	A1B/2050	9.3%
Döll (2002)	Various	ET_c – P	No	IS92a/2020	+5-20%
Fischer et al. (2007)	Various	AEZ	Yes	A2/2040	+10%
Iglesias and Minguez (1997)	Corn	CERES	Yes	+600 μmol^{-1}	+3 to +8%
Rey et al. (2011)	Corn	CERES	Yes	A2 /2070	−3%[c]
Jorge and Ferreres (2001)	Corn and Sunflower	CropWat	No	A/2050	+7.5%

[a] The method used in this paper "ET_c – P" is described in Section 5. Döll (2002) uses a similar method, described in their paper. CERES is described in Jones and Kiniry (1986), CropWat in Smith (1993) and AEZ in Fischer et al. (2005).
[b] The emission scenarios A1B, A2 and A are presented in Nakićenović et al. (2000) and IS92a in Leggett et al. (1992). Scenarios in Iglesias and Minguez (1997) are defined by an increase in temperature (1 or 3 °C) or CO_2 concentration (+600 μmol^{-1}).
[c] Before impact of precipitation changes. Precipitation decreases of about 14% in summer (based on the average of the four RCM), which results in an irrigation increase of about 6% with an irrigation of 200 mm/year in present climate.

needs. In the fourth scenario, when expanding crops with a lower water use, the decrease in irrigation needs is between 12% and 15% in the future climate, compared to the current situation.

6. Results from the hydrological simulations

In this section, we analyze the outputs of the different hydrological simulations. These results are based on the hydrological model presented in Section 3. Climate and irrigation inputs are discussed in Sections 4 and 5. Our comparison concentrates on the differences in the hydrological responses of the catchment to climate change, distinguishing between the four irrigation scenarios. We investigate the responses of hydraulic head, base flow, peak flow, and actual evapotranspiration.

6.1. Overview of the water balance

In Fig. 8, we briefly present the yearly water balance of the catchment in scenario 1 (non-irrigated) and scenario 2 (present irrigation) in the present climate. We analyze the individual parts of the water balance in the subsequent sections. Hence, this section only gives a general introduction.

In the Lerma catchment, precipitation is the main water input to the catchment, closely followed by irrigation (350 mm/year and 222 mm/year, respectively). In the lower portion of the catchment, where most of the irrigation is applied, irrigation input exceeds precipitation.

Actual evapotranspiration is the main water loss (about 261 mm/year in Scenario 1 without irrigation) and it increases by 56% if irrigation is present. Discharge is a small part of the water balance in this catchment. It increases in the irrigated cases, reaching 110 mm/year, but it stays noticeably under the actual evapotranspiration volume in all scenarios. Because of the critical depth boundary condition in the surface catchment, precipitation and irrigation which fall outside of the surface catchment but inside the boundary of the aquifer can freely leave the domain (see Section 3.1). This water volume

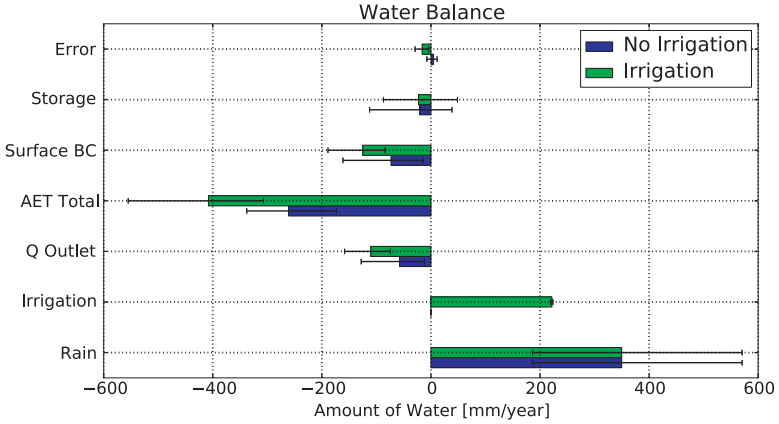

Fig. 8. Water balance of the catchment in the irrigated (Scenario 2) and non-irrigated cases (Scenario 1) for the present climate. See Section 6.1 for the definition of the "Surface BC" component. The error bars represent the spread of the 30 realizations created with the weather generator.

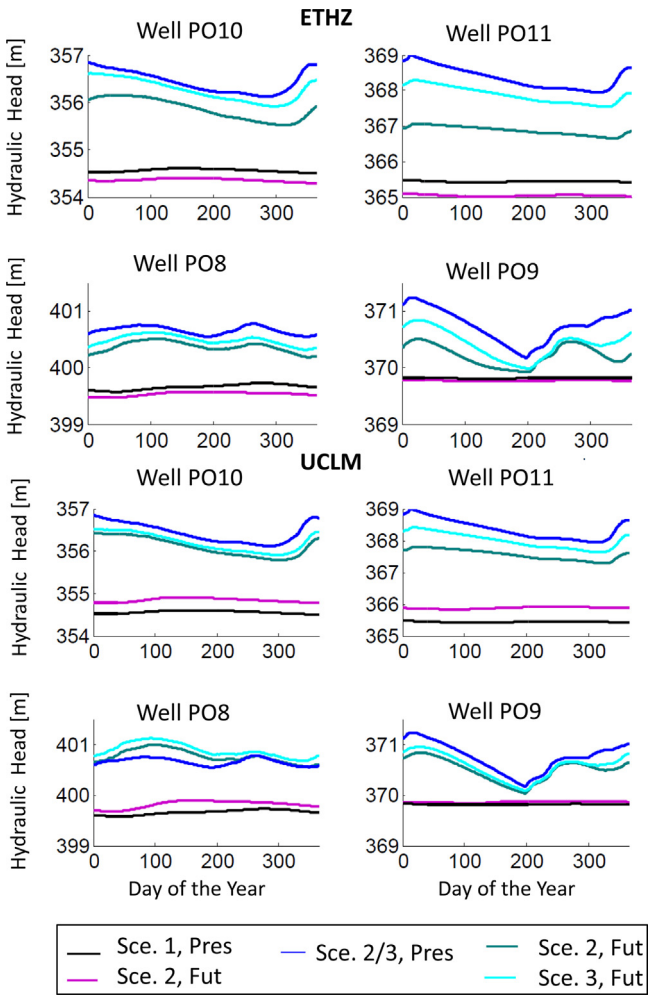

Fig. 9. Daily hydraulic heads in four wells for the scenarios 1 (no irrigation), 2 (present irrigation), and 3 (future irrigation) for the 30 realizations of the weather generator. Average over the 6 hydraulic years and over the 30 realizations (Start: 1st of October).

is indicated by the name "Surface BC" in Fig. 8 and it increases in scenario 2 (with irrigation) because of the additional water volume which enters the fields which are outside of the surface catchment.

Storage is similar with and without irrigation (about −20 mm/year). This storage is not the storage change from the "non-irrigated" (scenario 1) to the "irrigated" (scenario 2) stage. The latter would be larger and positive. The storage indicated in Fig. 8 would be zero on average if the catchment was at steady state. However, the meteorological measurements which inform the weather generator end in 2011. This means that parts of the measurements show a small but noticeable increase in temperature, consistent with the current climate change in the region. Hence, the current climate has a small drying effect on the catchment because of the increase in reference evapotranspiration. However, the storage change is small and close to the model error.

6.2. Hydraulic heads

Fig. 9 shows yearly time series of predicted hydraulic heads (i.e., groundwater level) in four observation wells for the scenarios with no irrigation, present, and future irrigation (scenarios 1, 2, and 3 from Section 5) for the regional climate models ETHZ and UCLM. Hydraulic heads driven by the climate scenarios based on MPI are showing similar results to those based on UCLM and hydraulic heads driven by the climate scenarios based on METO are similar to those based on ETHZ. Consequently, the results of the MPI and METO regional climate models are not shown here for brevity.

Under present climate conditions, predicted groundwater levels are higher when the catchment is irrigated than when it is not. The maximum mean difference is 2.7 m in the observation well PO11 (Fig. 1) but is about 1m for most observation wells, which is consistent with the observed changes during the transition to irrigation. Each observation well responds differently to the irrigation onset. Generally, irrigation seems to strongly affect the wells which are located in the thickest

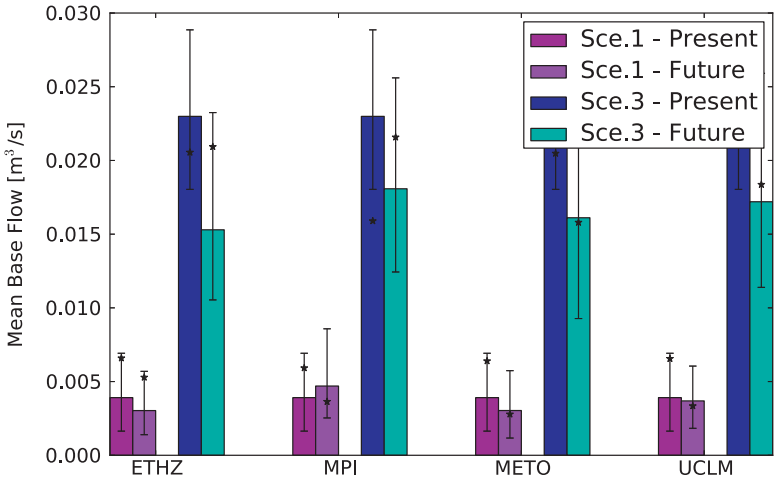

Fig. 10. Present and future base flow in the scenarios without irrigation (Scenario 1) and with future irrigation (Scenario 3). The error bars represent the spread of the 30 scenarios created with the weather generators. The stars indicate the results using the quantile mapped downscaling method.

part of the aquifer (e.g, PO11). Moreover, if a well is close to the aquifer boundaries (such as PO9), its response to irrigation is often less directly related to this impulse because the groundwater flow is affected by the aquifer boundaries.

Hydraulic heads generally decline from present to future climate. The extent of the decrease in hydraulic heads depends on the precipitation outputs of the regional climate models. Two regional climate models (ETHZ and METO) predict a decrease in annual precipitation and two regional climate models (MPI and UCLM) predict an increase in annual precipitation, when compared to the present situation. If the annual precipitation is predicted to decrease, hydraulic heads strongly decrease in all wells. If the annual precipitation is predicted to increase, hydraulic heads often decrease nonetheless, because of the increased ET_c and changes in precipitation seasonality. However, if annual precipitation is predicted to increase, the decrease in hydraulic head is smaller and even an increase in hydraulic head is observed in some wells. In the observation wells PO9, PO10, and PO11 for scenario 2, future hydraulic heads decrease (between 1.3 m and 0.13 m, depending on the wells), regardless of the regional climate model. Nevertheless, the decrease is about 2 times smaller when UCLM or MPI is used instead of ETHZ or METO. Moreover, the predicted mean hydraulic head in the observation well PO8 in scenario 2 (present irrigation) is 0.1 m higher in the UCLM climate scenario than in the present climate. The hydraulic head in this well decreases by 0.25 m when the ETHZ climate scenario is compared to the present level (average of daily data, based on the 30 hydrological simulations). The weaker response of well PO8 to climate change (when compared to other observation wells) may be an artifact of the hydrological model as it underestimates the variability of hydraulic head in this well already under current climate conditions (see the corresponding results of the calibration and validation periods in Fig. 4).

Generally, the impacts of climate change on groundwater levels are larger in the scenarios with irrigation (scenarios 2, 3 and 4) than in the scenario without irrigation (scenario 1). This is particularly true for scenario 2 (present irrigation) because the higher irrigation demand, lower precipitation, and higher ET_c result in a generally decreasing water table. Differences between present and future groundwater levels are nevertheless larger in scenario 3 (future climate and irrigation) than in the scenario 1 (without irrigation). In general, in scenario 1, hydraulic heads decrease only little (about 0.18 m with the ETHZ or METO climate scenarios) or increase only slightly (about 0.15 m, when using MPI or UCLM climate scenario). When irrigation is present, the decrease can be about 1.3 m in Scenario 2 or about 0.4 m in scenario 3 (observation well PO11 in the ETHZ climate scenario).

The increased sensitivity of groundwater levels to climate change in the scenarios with irrigation (2 and 3) is probably a consequence of the higher water table, increased transpiration, soil moisture, and deeper root depth, which are a result of the irrigation onset. The dependence between groundwater levels and climate processes increases when the water table is closer to the surface, especially if the root depth is close to the water level (Kollet and Maxwell, 2008). The mean depth to groundwater in the north of the domain decreased from about 3.7 m prior to irrigation (2005) to about 2.6m after the transition to irrigation (2011). The model considers the root depth (the maximum depth at which plants extract water for transpiration), as a spatially distributed parameter. It is chosen to be 1m for corn (which is the main crop in the catchment) and 0.1 m for uncultivated soil. Hence, the mean distance from the water table to the bottom of the root zone passes from 3.6 m to 1.6 m after irrigation started in the catchment, resulting in a better connection between the water table and the root zone. This range is within the critical depth identified by Kollet and Maxwell (2008) where evapotranspiration is sensitive to the water-table depth. In addition to the decreased depth to the water table, the larger soil moisture results in a higher sensitivity of actual evapotranspiration to ET_c, resulting in a higher sensitivity of recharge to ET_c-changes, and therefore of the groundwater levels to climate change.

6.3. Base flow

In this study, we define base flow as total discharge in days with no precipitation on this day and the previous day. Because of the large hydraulic conductivity of the aquifer and the small size of the Lerma catchment, discharge peaks generally recess in less than a day. Therefore, the total discharge during the periods with no precipitation largely depends on subsurface flow and is a good estimation of base flow. Base flow has similar responses to changes in irrigation and climate as groundwater levels (Fig. 10). In present climate, average daily base flow is 5.8 times higher in presence of irrigation than without. This is similar to the measured response of discharge to irrigation onset. Measured base flow was about 5.2 times larger in the hydrological year 2011 (after the implementation of irrigation) than in 2006 (before the start of irrigation), corresponding to an increase in flow of about 0.015 m^3/s. The measured annual precipitation was lower in 2011 (365 mm) than in 2006 (459 mm).

When comparing present and future climate, base flow decreases more in scenarios with irrigation, i.e., scenarios 2, 3, and 4, than in scenario 1 without irrigation. In scenario 3 (with future irrigation), the decrease of mean daily base flow due to climate change is between 33% and 21% of the present base flow, or $-0.008\ m^3/s$ and $-0.005\ m^3/s$, depending on the used regional climate model (average on all hydrological simulations). In scenario 1 (without irrigation), future daily base flow decreases between $-9\times10^{-4}\ m^3/s$ and $-2\times10^{-4}\ m^3/s$ for the ETHZ, UCLM, and METO climate scenarios and increases of $8\times10^{-4}\ m^3/s$ in the MPI climate scenario. Fig. 10 shows the mean base flow using the four regional climate models for the scenario with no irrigation and future irrigation (Scenarios 1 and 3).

6.4. Peak discharge

On the regional scale, flood risk is low in the Ebro region because of the various reservoirs, that control river flows and cap peak flows (Bovolo et al., 2010). However, flood protection might fail if intense precipitation events occur in rapid succession (López-Moreno et al., 2002) and is not always effective on a local scale, where streamflow depends more on local precipitation events. Moreover, the variability of precipitation is predicted by all regional climate models to increase moderately in the spring and possibly during summer (UCLM and METO, see Fig. 6). This higher variability might increase future peak discharges.

However, the relation between precipitation events and corresponding discharge responses is not linear and depends notably on prior soil moisture conditions (Hill et al., 2010). In the Lerma catchment, before the introduction of irrigation, the soil was generally relatively dry and covered by sparse vegetation. Consequently, during intense convective rainfall events, run-off generation was primarily controlled by the infiltration rate (Pérez et al., 2011). When irrigation was introduced in the Lerma catchment, soil moisture increased and cultivation changed the soil characteristics. These transformations had a strong influence on the run-off generation mechanisms and annual peak discharge decreased. When considering the average of all hydrological simulations in present climate, mean annual maximum daily discharge is 1.42 m^3/s in scenario 1, without irrigation, and 0.55 m^3/s in the scenarios with irrigation, a 61% decrease. A similar behavior is observed in the measured time series of discharge and has often been noticed in catchments with a semi-arid climate (e.g., Berndtsson and Larson, 1987).

After calibration, our model is able to adequately reproduce these changes. Indeed, because of the fine vertical layering (about 1–3 cm close to the surface), the model allows for a rapid saturation of the surface and shallow subsurface zones (during an event with a large precipitation intensity) and a delayed vertical water movement under low-saturation conditions. Additionally, soil parameters are different for each soil zone, influencing infiltration and peak discharges (Fig. 2). Finally, surface flow velocities are faster when crops are absent because of a lower surface roughness, resulting in a shorter contact time and a lower infiltration in the scenario without irrigation.

Fig. 11 presents the annual daily maximum flow, based on the present and future climate predicted by all regional climate models. Annual maximum flows increase when the coefficient of variation of precipitation is predicted to increase in summer (UCLM and METO), a period of frequent intense precipitation events. The increase is relatively small when comparing the median annual maximum flow over all hydrological simulations. For example, in scenario 1, the median annual peak discharge shows an increase of 0.12 m^3/s (8.7%) in the METO case. However, when considering the years with an annual maximum discharge in the higher quartile, the increase is more important, especially in scenario 1 (without irrigation). In this scenario, when considering the years with an annual maximum peak flow in the higher quartile, the annual maximum discharges show an increase of 0.5 m^3/s (29%) in the METO climate scenario and of 1.24 m^3/s (68%) in the UCLM climate scenario. In scenario 3 (future irrigation), the annual maximum flows in the higher quartile increase, but only moderately. In the METO climate scenario, the increase amounts to 0.13 m^3/s. Therefore, without irrigation, changes in precipitation variability in summer, which are linked with an increase in intense precipitation events, have a large impact on peak discharge. When changes in precipitation variability is unclear or when precipitation variability decreases in summer (MPI and ETHZ), annual maximum flow is not showing a clear trend (Fig. 11). Results are similar for all irrigation scenarios (2, 3, and 4).

6.5. Actual evapotranspiration

All regional climate models predict an increase in ET_c. However, because of soil-moisture limitations, this does not automatically imply an increase in actual evapotranspiration (AET). For example, in scenario 1 (without irrigation), future

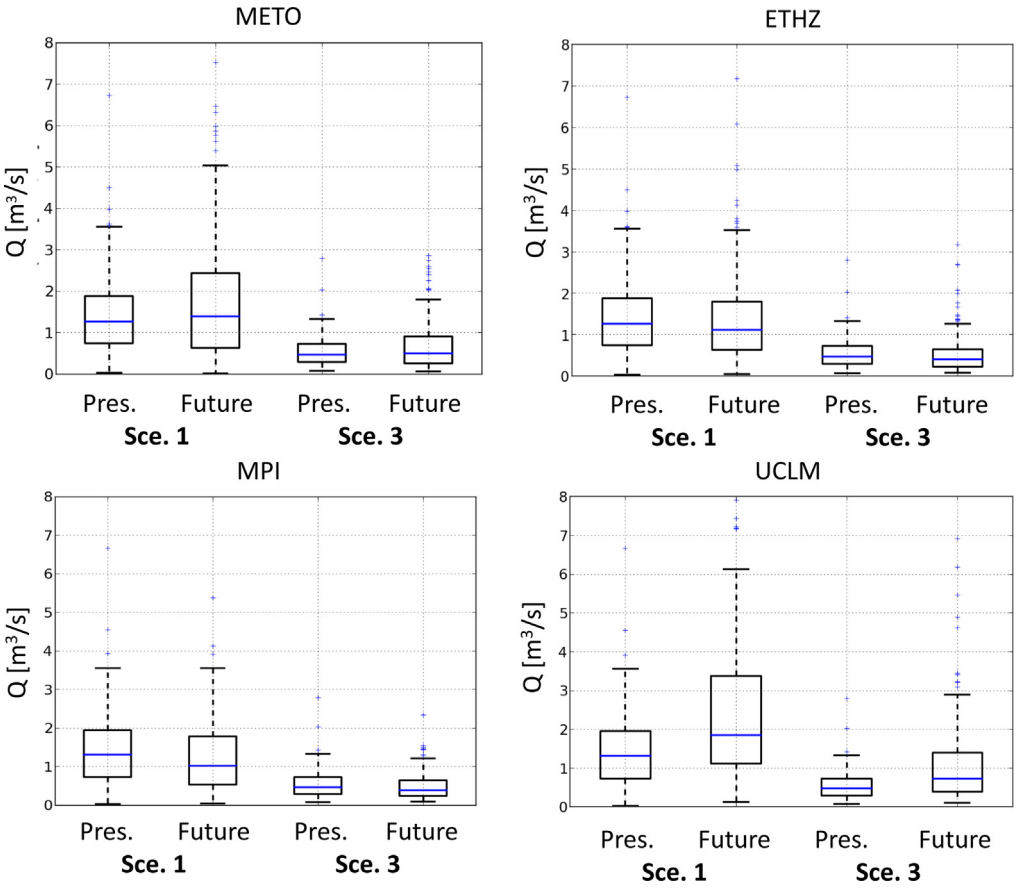

Fig. 11. Annual maximum outflow for the four regional climate models. Scenario 1 (with no irrigation) and 3 (future irrigation).

AET decreases during summer for all climate scenarios (Fig. 12). In general, in scenario 1 (no irrigation), changes in ET_c have a small impact and changes in AET follow the precipitation changes. Climate scenarios based on regional climate models predicting a large decrease in summer precipitation as ETHZ (−36% of present precipitation) forecasts a relatively large decrease in AET (−27% of present AET). On the contrary, if the regional climate model predicts only small changes in summer precipitation (e.g., MPI with −6% of present precipitation), AET does not decrease as much (−3.3% of present AET).

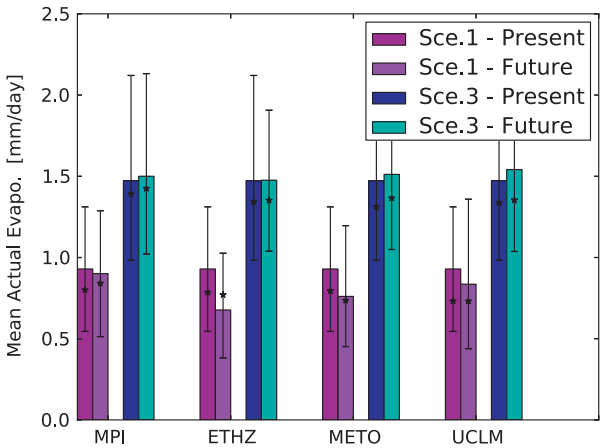

Fig. 12. Present and future AET in the scenarios without irrigation and with future irrigation during the irrigation period (15th April to 30th September). The error bars represent the spread of the 30 scenarios created with the weather generators. The stars indicate the results using the quantile mapped downscaling method.

On the contrary, with irrigation, soil moisture increases and AET increases during summer because of the higher water availability (Fig. 12). When comparing the situation in present climate, AET is 56% larger when fields are irrigated compared to a situation without irrigation. In future climate with irrigation, especially in scenario 3, AET increases, contrarily to the results based on scenario 1 (without irrigation). In scenarios 2 and 3, the future increase in ET_0 has more impact on AET than in scenario 1 because of the generally larger soil moisture. However, the differences in AET between future and present climate are still relatively small (between 0.003 mm/day and 0.07 mm/day).

In the scenario with future cropping patterns (scenario 4), yearly AET is predicted to decrease by 8% in the ETHZ case, when compared to the present cropping pattern and climate (scenario 2, present). AET is strongly impacted by water availability in semi-arid climates and total irrigation volume in scenario 4 is about 15% smaller (Section 5.2) than in the present case. However, the decrease of AET in this scenario is predicted to occur mainly in summer, during the vegetative period, when AET has its seasonal peak. Future AET in winter increases of 20%, due to the higher irrigation, precipitation and transpiration during this period. Indeed, in scenario 4, the area where winter cereal is cultivated increases, resulting in an overall higher transpiration in the catchment during the cultivation period of this crop.

7. Discussion and conclusion

Water availability will likely decrease in the Ebro region (Bovolo et al., 2010) as a result of climate change. An increase of the irrigation demands by about 10% (Table 7 and Section 5.2) is predicted in the next 40 years in the Ebro region, based on current cropping practices. In addition, the volume of water available for storage in the Yesa reservoir, which is the water source for irrigation in the Lerma catchment, will probably decrease. For example, López-Moreno et al. (2014) modeled a 30% decrease of streamflow to the Yesa reservoir, because of land-use and climate change. Moreover, an expansion of the irrigated area (between 30% and 50% of the present irrigated area) is currently planned by the local irrigation authority in the region (Bielsa and Cazcarro, 2015; Milano et al., 2013). Consequently, efficient mitigation strategies for climate change impacts are needed. These strategies should consider land-use changes and future agricultural practices. As demonstrated by this study, the impact of climate change will be different for irrigated and non-irrigated areas. For example, annual maximum peak flow could increase more in non-irrigated regions compared to irrigated regions. Consequently, flood risk increases more in non-irrigated areas than in irrigated areas, even with identical changes in precipitation variability.

In contrast, base flow rates are more impacted by climate change in streams which are heavily influenced by irrigated agriculture. In the Lerma catchment, the transition from rain-fed to irrigation agriculture has resulted in larger flows in the streams during dry periods because of higher groundwater levels. However, stream flows are expected to decrease under future climate scenarios. Base flows in irrigated catchments might therefore rapidly change. This change is expected to impact, for example, stream ecology, as rapid changes of flow rate are difficult to overcome by ecological communities (e.g Sandel et al., 2011; Bradford and Heinonen, 2008), or on water quality as lower outflows might results in an increase of nutriment and pollutant concentrations (Whitehead et al., 2009), because of the lacking dilution.

In semi-arid climates, the actual evapotranspiration (AET) on the catchment scale depends on water availability in the soil zone, among other factors. In the Lerma basin, climate change is predicted to result in a decrease of AET in our scenario without irrigation but in an increase of AET in the scenarios where the catchment is irrigated in summer, especially for scenarios with increased irrigation volume. In this case, irrigation influences the gradient of air humidity, creating a feed-back loop between irrigation management and atmospheric conditions. Hence, impact of water management, as irrigation management, and climate changes are strongly interlinked and feed-backs between them should be analyzed and understood in climate-change impact studies (Holman, 2005).

Acknowledgments

This study was performed within the International Research Training Group “Integrated Hydrosystem Modelling” under the grant GRK 1829/1 funded by Deutsche Forschungsgemeinschaft (DFG). We acknowledge the ENSEMBLES project, funded by the European Commission’s 6th Framework Programme through contract GOCE-CT-2003-505539. The support of the Spanish meteorological national agency (AEMET) is here gratefully acknowledged too. Research in the Lerma catchment is supported by the grant CGL-2012-32395 (Spanish Ministry of Economy and Competitiveness and European Union, FEDER funds). Daniel Merchán was sponsored by the BES2010-034124 grant of the Spanish Ministry of Economy and Competitiveness. We thank as well H.Fowler and S.Blenkinsop for their support and for providing the weather generators.

Appendix A. Supplementary Data

Supplementary data associated with this article can be found, in the online version, at http://dx.doi.org/10.1016/j.ejrh.2015.08.001.

References

Abrahao, R., Causapé, J., García-Garizábal, I., Merchán, D., 2011. Implementing irrigation: water balances and irrigation quality in the Lerma basin (Spain). Agric. Water Manage. 102, 97–104.

Allen, R., Pereira, L., Raes, D., Smith, M., 2000. Crop evapotranspiration (guidelines for computing crop water requirements). FAO irrigation and drainage paper 56.
Beltrán, A., 1986. Estudio de los suelos de la zona regable de Bardenas II. Sectores VIII, IX, X, XII y XIII. Instituto Nacional de Reforma y Desarrollo Agrario, Ministerio de Agricultura, Pesca y Alimentación.
Berndtsson, R., Larson, M., 1987. Spatial variability of infiltration in a semi-arid environment. J. Hydrol. 90, 117–133.
Bielsa, J., Cazcarro, I., 2015. Implementing integrated water resources management in the Ebro river basin: from theory to facts. Sustainability 7, 441–464.
Blenkinsop, S., Fowler, H., 2007. Changes in European drought characteristics projected by the PRUDENCE regional climate models. Int. J. Climatol. 27, 1595–1610.
Bouraoui, F., Vachaud, G., Li, L., le Treut, H., Chen, T., 1999. Evaluation of the impact of climate changes on water storage and groundwater recharge at the watershed scale. Clim. Dyn. 15, 153–161.
Bovolo, C., Blenkinsop, S., Majone, B., Zambrano-Bigiarini, M., Fowler, H., Bellin, A., Burton, A., Barceló, D., Grathwohl, P., Barth, J., 2010. Climate change, water resources and pollution in the Ebro basin: Towards an integrated approach. In: Barceló, D., Petrovic, M. (Eds.), The Ebro River Basin. Springer-Verlag.
Bradford, M., Heinonen, J., 2008. Low flows, instream flow needs and fish ecology in small streams. Can. Water Resour. J. 33, 165–180.
Buerger, C., Kolditz, O., Fowler, H., Blenkinsop, S., 2007. Future climate scenarios and rainfall-runoff modelling in the Upper Gallego catchment (Spain). Environ. Pollut. 148, 842–854.
Burton, A., Fowler, H., Blenkinsop, S., Kilsby, C., 2010. Downscaling transient climate change using a Neyman-Scott rectangular pulses stochastic rainfall model. J. Hydrol. 381, 18–32.
Burton, A., Kilsby, C., Fowler, H., Cowpertwait, P., O'Conell, P., 2008. RainSim: a spatial-temporal stochastic rainfall modelling system. Environ. Model. Softw. 23, 1356–1369.
Candela, L., von Igel, W., Elorza, F.J., Aronica, G., 2009. Impact assessment of combined climate and management scenarios on groundwater resources and associated wetland (Majorca, Spain). J. Hydrol. 376, 510–527.
Candela, L., Tamoh, K., Olivares, G., Gomez, M., 2012. Modelling impacts of climate change on water resources in ungauged and data-scarce watersheds. Application to the Siurana catchment (NE Spain). Sci. Total Environ. 440, 253–260.
Christensen, J., Christensen, O., 2007. A summary of the PRUDENCE model projections of changes in European climate by the end of this century. Clim. Change 81, 7–30.
Christensen, O., Drews, M., Christensen, J., Dethloff, K., Ketelsen, K., Hebestadt, I., Rinke, A., 2006. The HIRHAM regional climate model version 5 (b), tech. rep. 06-17. Dan. Meteorol. Inst., Copenhagen.
Collins, M., Booth, B., Harris, G., Murphy, J., Sexton, D., Webb, M., 2006. Towards quantifying uncertainty in transient climate change. Clim. Dyn. 27, 127–147.
Cuo, L., Zhang, Y., Gao, Y., Hao, Z., Cairang, L., 2013. The impacts of climate change and land cover/use transition on the hydrology in the upper Yellow River Basin, China. J. Hydrol. 502, 37–52.
Dale, V., 1997. The relationship between land-use change and climate change. Ecol. Appl. 7, 753–769.
Döll, P., 2002. Impact of climate change and variability on irrigation requirements: a global perspective. Clim. Change 54, 269–293.
Ferrer, J., Pérez-Martín, M.A., Jiménez, S., Estrela, T., Andreu, J., 2012. GIS-based models for water quantity and quality assessment in the Júcar river basin, Spain, including climate change effects. Sci. Total Environ. 440, 42–59.
Fischer, G., Shah, M., Tubiello, F., van Velhuizen, H., 2005. Socio-economic and climate change impacts on agriculture: an integrated assessment, 1990–2080. Philos. Trans. R. Soc. 360, 2067–2083.
Fischer, G., Tubiello, F., van Velthuizen, H., Wiberg, D., 2007. Climate change impact on irrigation water requirements. effects of mitigation, 1990–2080. Technol. Forecast. Soc. Change 74, 1083–1107.
Flato, G., Marotzke, J., Abiodun, B., Braconnot, P., Chou, S., Collins, W., Cox, P., Driouech, F., Emori, S., Eyring, V., Forest, C., Gleckler, P., Guilyardi, E., Jakob, C., Kattsov, V., Reason, C., Rummukainen, M., 2013. Evaluation of climate models. In: Climate change 2013: The physical science basis. Contribution of working group I to the fifth assessment report of the intergovernmental panel on climate change. Cambridge University Press, Cambridge, United Kingdom and New York, NY, USA.
Fowler, H., Blenkinsop, S., Tebaldi, C., 2007. Linking climate change modelling to impacts studies: recent advances in downscaling techniques for hydrological modelling. Int. J. Climatol. 27, 1547–1578.
Fujihara, Y., Tanaka, K., Watanabe, T., Nagano, T., Kojiri, T., 2008. Assessing the impacts of climate change on the water resources of the Seyhan river basin in Turkey: use of dynamically downscaled data for hydrologic simulations. J. Hydrol. 353, 33–48.
García-Garizábal, I., Causapé, J., 2010. Influence of irrigation water management on the quantity and quality of irrigation return flows. J. Hydrol. 385, 36–43.
García-Garizábal, I., Causapé, J., Abrahao, R., Merchán, D., 2014. Impact of climate change on Mediterranean irrigation demand: Historical dynamics of climate and future projections. Water Resour. Manage. 28, 1449–1462.
Ghosh, S., Misra, C., 2010. Assessing hydrological impacts of climate change: modeling techniques and challenges. Open Hydrol. J. 4, 115–121.
Goderniaux, P., Brouyère, S., Blenkinsop, S., Burton, A., Fowler, H.J., Orban, P., Dassargues, A., 2011. Modeling climate change impacts on groundwater resources using transient stochastic climatic scenarios. Water Resour. Res. 47, W12516.
Goderniaux, P., Brouyère, S., Fowler, H., Blenkinsop, S., Therrien, R., Orban, P., Dassargues, A., 2009. Large scale surface-subsurface hydrological model to assess climate change impacts on groundwater reserves. J. Hydrol. 373, 122–138.
Haugen, J., Haakenstad, H., 2006. Validation of HIRHAM version 2 with 50 km and 25 km resolution. RegClim Phase III – Gen. Tech. Rep. 9. Norw. Meteorol. Inst., Oslo.
Herrera, S., Fita, L., Fernández, J., Gutiérrez, J.M., 2010. Evaluation of the mean and extreme precipitation regimes from the ENSEMBLES regional climate multimodel simulations over Spain. J. Geophys. Res. 115, D21117.
Hewitt, C., Griggs, D., 2004. Ensembles-based predictions of climate changes and their impacts. Trans. Am. Geophys. Union (EOS) 85, 556.
Hill, C., Verjee, F., Barrett, C., 2010. Flash flood early warning system reference guide. National Oceanic and Atmospheric Administration, U.S. Department of Commerce.
Hill, M., Tiedeman, C., 2007. Effective Groundwater Model Calibration: With Analysis of Data, Sensitivities, Predictions, and Uncertainty. John Wiley and Sons, Inc.
Holman, I., 2005. Climate change impacts on groundwater recharge-uncertainty, shortcomings, and the way forward? Hydrogeol. J. 14, 637–447.
Holman, I., Tascone, D., Hess, T., 2009. A comparison of stochastic and deterministic downscaling methods for modelling potential groundwater recharge under climate change in East Anglia, UK: implications for groundwater resource management. Hydrogeol. J. 17, 1629–1641.
Iglesias, A., Minguez, M., 1997. Modelling crop-climate interactions in Spain: vulnerability and adaptation of different agricultural systems to climate change. Mitig. Adapt. Strateg. Glob. Changes 1, 273–288.
I.G.N., 2012. Modelo Digital del Terreno, hoja 282 del Mapa Topográfico Nacional (in Spanish). Instituto Geográfico Nacional.
Jacob, D., Van den Hurk, B., Andrae, U., Elgered, G., Fortelius, C., Graham, L.P., Jackson, S.D., Karstens, U., Köpken, C., Lindau, R., Podzun, R., Rockel, B., Rubel, F., Sass, B.H., Smith, R.N.B., Yang, X., 2001. A comprehensive model inter-comparison study investigating the water budget during the BALTEX-PIDCAP period. Meteorol. Atmos. Phys. 77, 19–43.
Jaeger, E., Anders, I., Lüthi, D., Rockel, B., Schär, C., Seneviratne, S., 2008. Analysis of ERA40-driven CLM simulations for Europe. Meteorol. Ztg. 17, 349–367.
Jones, C., Kiniry, J., Dyke, P., 1986. CERES-maize: A simulation model of maize growth and development. Texas A. and M. University Press, pp. 194.
Jorge, J., Ferreres, E., 2001. Irrigation scenario vs climate change scenario. In: India, M., Bonillo, D. (Eds.), Detecting and Modelling Regional Climate Change. Springer, Berlin/Heidelberg, pp. 581–592.
Kilsby, C., Jones, P., Burton, A., Ford, A., Fowler, H., Harpham, C., James, P., Smith, A., Wilby, R., 2007. A daily weather generator for use in climate change studies. Environ. Model. Softw. 22, 1705–1719.

Kjellström, E., Bärring, L., Gollvik, S., Hansson, U., Jones, C., Samuelsson, P., Rummukainen, M., Ullerstig, A., Willén, U., Wyser, K., 2005. A 140-year simulation of European climate with the new version of the Rossby Centre regional atmospheric climate model (RCA3). Rep. Meteorol. Climatol. Swed. Meteorol. and Hydrol. Inst., Norrköping, Sweden, pp. 54.
Kling, H., Stanzel, P., Preishuber, M., 2014. Impact modelling of water resources development and climate scenarios on Zambezi River discharge. J. Hydrol. Reg. Stud. 1, 17–43.
Kollet, S., Maxwell, R., 2008. Capturing the influence of groundwater dynamics on land surface processes using an integrated, distributed watershed model. Water Resour. Res. 44, W02402.
Kubatzki, C., Claussen, M., Calov, R., Ganopolski, A., 2006. Sensitivity of the last glacial inception to initial and surface conditions. Clim. Dyn. 27, 333–344.
Leggett, J., Pepper, W., Swart, R., 1992. Emission scenarios for the IPCC: An update – the supplementary report to the IPCC scientific assessment. Cambridge University Press.
Li, H., Sheffield, J., Wood, E., 2009. Bias correction of monthly precipitation and temperature fields from intergovernmental panel on climate change AR4 models using equidistant quantile matching. J. Geophys. Res. 115, D10101.
van der Linden, P., Mitchell, J., 2009. ENSEMBLES: climate change and its impact: summary of research and results from the ENSEMBLES project. Met Office Hadley Centre, UK, pp. 1–160.
López-Moreno, J., Beguería, S., García-Riuz, J., 2002. Influence of the Yesa reservoir on floods of the Aragón river, central Spanish Pyrenees. Hydrol. Earth Sys. Sci. 6, 753–762.
López-Moreno, J., Zabalza, J., Vicente-Serrano, S., Revuelto, J., Gilaberte, M., Azorin-Molina, C., Morán-Tejeda, E., García-Ruiz, J., Tague, C., 2014. Impact of climate and land use change on water availability and reservoir management: Scenarios in the Upper Aragón river, Spanish Pyrenees. Sci. Total Environ. 493, 1222–1231.
Martínez-Cob, A., 2004. Revisión de las necesidades hídricas netas de los cultivos de la cuenca del Ebro. Confederación Hidrográfica del Ebro.
Meehl, G.A., Stocker, T.F., et al., 2007. Global climate projections. In: Climate Change 2007: The Physical Science Basis. Contribution of Working Group I to the Fourth Assessment Report of the Intergovernmental Panel on Climate Change. Cambridge University Press, Cambridge.
Mehdi, B., Ludwig, R., Lehner, B., 2015. Evaluating the impacts of climate change and crop land use change on streamflow, nitrates and phosphorus: a modeling study in Bavaria. J. Hydrol. Reg. Stud. Part B 4, 60–90.
Mehta, V.K., Haden, V.R., Joyce, B.A., Purkey, D.R., Jackson, L.E., 2013. Irrigation demand and supply, given projections of climate and land-use change, in Yolo County, California. Agr. Water Manage. 117, 70–82.
van Meijgaard, E., van Ulft, L., van de Berg, W., Bosveld, F., van den Hurk, B., Lenderink, G., Siebesma, A., 2008. The KNMI regional atmospheric climate model RACMO, version 2.1, KNMI – tech. rep. 302.
Merchán, D., Causapé, J., Abrahao, R., 2013. Impact of irrigation implementation on hydrology and water quality in a small agricultural basin in Spain. Hydrolog. Sci. J. 58, 1400–1413.
Merchán, D., Otero, N., Soler, A., Causapé, J., 2014. Main sources and processes affecting dissolved sulphates and nitrates in a small irrigated basin (Lerma basin, Zaragoza, Spain): isotopic characterization. Agr. Ecosyst. Environ. 195, 127–138.
Milano, M., Ruelland, D., Dezetter, A., Fabre, J., Ardoin-Bardin, S., Servat, E., 2013. Modeling the current and future capacity of water resources to meet water demands in the Ebro basin. J. Hydrol. 500, 114–126.
Montenegro, S., Ragab, R., 2012. Impact of possible climate and land use changes in the semi arid regions: a case study from North Eastern Brazil. J. Hydrol. 434–435, 55–68.
Moratiel, R., Durán, J., Snyder, R., 2010. Responses of reference evapotranspiration to changes in atmospheric humidity and air temperature in Spain. Clim. Res. 44, 27–40.
Moussa, R., Bocquillon, C., 2000. Approximation zones of the Saint-Venant equations for flood routing with overbank flow. Hydrol. Earth Syst. Sci. 4, 251–261.
Nakićenović, N., Davidson, O., Davis, G., Grübler, A., Kram, T., Rovere, E.L.L., Metz, B., Morita, T., Pepper, W., Pitcher, H., Sankovski, A., Shukla, P., Swart, R., Watson, R., Dadi, Z., 2000. Emissions scenarios – summary for policymakers. A special report of working group III of the Intergovernmental Panel on Climate Change.
Nash, J., Sutcliffe, V., 1970. River flow forecasting through conceptual models, part I – a discussion of principles. J. Hydrol. 10, 282–290.
Ntegeka, V., Baguis, P., Roulin, E., Willems, P., 2014. Developing tailored climate change scenarios for hydrological impact assessments. J. Hydrol. 508, 307–321.
Otero, I., Boada, M., Badia, A., Pla, E., Vayreda, J., Sabaté, S., Gracia, C.A., Peñuelas, J., 2011. Loss of water availability and stream biodiversity under land abandonment and climate change in a Mediterranean catchment (Olzinelles, NE Spain). Land Use Policy 28, 207–218.
Pal, J., Giorgi, F., Bi, X., Elguindi, N., Solmon, F., Rauscher, S.A., Gao, X., Francisco, R., Zakey, A., Winter, J., Ashfaq, M., Syed, F.S., Sloan, L.C., Bell, J.L., Diffenbaugh, N.S., Karmacharya, J., Konaré, A., Martinez, D., da Rocha, R.P., Steiner, A.L., 2007. Regional climate modeling for the developing world: the ICTP regCM3 and regCNET. Bull. Am. Meterol. Soc. 88, 1395–1409.
Pérez, A., 2011. Physics-based numerical modeling of surface-groundwater flow and transport at catchment scale. University of Tübingen (Ph.D. thesis).
Pérez, A., Abrahao, R., Causapé, J., Cirpka, O., Bürger, C., 2011. Simulating the transition of a semi-arid rainfed catchment towards irrigation agriculture. J. Hydrol. 409, 663–681.
Pielke, R., 2005. Land use and climate change. Science 310, 1625–1626.
Plata-Torres, J., 2012. Informe sobre la campaña de sondeos eléctrico verticales efectuados en el barranco de Lerma (Zaragoza). Grupo de Geofísica del Instituto Geológico y Minero de España.
Radu, R., Déqué, M., Somot, S., 2008. Spectral nudging in a spectral regional climate model. Tellus Ser. A 60, 898–910.
Rey, D., Garrido, A., Mínguez, M., Ruiz-Ramos, M., 2011. Impact of climate change on maize's water needs, yields and profitability under various water prices in Spain. Span. J. Agric. Res. 9, 1047–1058.
Ribalaygua, J., Pino, M., Pórtoles, J., Roldán, E., Gaitán, E., Chinarro, D., Torres, L., 2013. Climate change scenarios for temperature and precipitation in Aragón (Spain). Sci. Total Environ. 463–464, 1015–1030.
Richards, L., 1931. Capillary conduction of liquids through porous mediums. J. Appl. Phys. 1, 318–333.
Sánchez, E., Gallardo, C., Gaertner, M., Arribas, A., Castro, M., 2004. Future climate extreme events in the Mediterranean simulated by a regional climate model: a first approach. Glob. Planet. Change 44, 163–180.
Sandel, B., Arge, L., Dalsgaard, B., Davies, R.G., Gaston, K.J., Sutherland, W.J., Svenning, J.C., 2011. The influence of late quaternary climate-change velocity on species endemism. Science 334, 660–664.
Scanlon, B.R., Jolly, I., Sophocleous, M., Zhang, L., 2007. Global impacts of conversions from natural to agricultural ecosystems on water resources: quantity versus quality. Water Resour. Res. 43, W03437.
Serrat-Capdevila, A., Scott, R., Shuttleworth, J., Valdés, J., 2011. Estimating evapotranspiration under warmer climates: insights from a semi-arid riparian system. J. Hydrol. 399, 1–11.
Sillmann, J., Roeckner, E., 2008. Indices for extreme events in projections of anthropogenic climate change. Clim. Change 86, 83–104.
Simonneaux, V., Cheggour, A., Deschamps, C., Mouillot, F., Cerdan, O., Le Bissonnais, Y., 2015. Land use and climate change effects on soil erosion in a semi-arid mountainous watershed (High Atlas, Morocco). J. Arid Environ. 122, 64–75.
Skhiri, A., Dechmi, F., 2011. Irrigation return flows and phosphorus transport in the Middle Ebro River valley (Spain). Span. J. Agric. Res. 9, 938–949.
Smith, M., 1993. CLIMWAT for CROPWAT: Climatic database for irrigation planning and management. FA0 Irrigation and Drainage Paper 49.
Szczypta, C., Gascoin, S., Houet, T., Hagolle, O., Dejoux, J.F., Vigneau, C., Fanise, P., 2015. Impact of climate and land cover changes on snow cover in a small Pyrenean catchment. J. Hydrol. 521, 84–99.
Tebaldi, C., Knutti, R., 2007. The use of the multi-model ensemble in probabilistic climate projections. Philos. Trans. R. Soc. 365, 2053–2075.

Therrien, R., 2006. HydroGeoSphere – A Three-Dimensional Numerical Model Describing Fully-Integrated Subsurface and Surface Flow and Solute Transport. Université Laval and University of Waterloo (Ph.D. thesis).
Therrien, R., McLaren, R., Sudicky, E., Panday, S., 2010. HydroGeoSphere: A Three-dimensional Numerical Model Describing Fully-integrated Subsurface and Surface Flow and Solute Transport – User Manual. University of Waterloo.
Toews, M., Allen, D., 2009. Evaluating different GCMs for predicting spatial recharge in an irrigated arid region. J. Hydrol. 374, 265–281.
Urdanoz, V., Aragüés, R., 2011. Pre- and post-irrigation mapping of soil salinity with electromagnetic induction techniques and relationships with drainage water salinity. Soil Sci. Soc. Am. J. 75, 207–215.
van Roosmalen, L., Sonnenborg, T., Jensen, K., Chistensen, J., 2011. Comparison of hydrological simulations of climate change using perturbation of observations and distribution-based scaling. Vadose Zone J. 10, 136–150.
van Genuchten, M., 1980. A closed-form equation for predicting the hydraulic conductivity of unsaturated soils. Soil Sci. Soc. Am. J. 44, 892–898.
von Gunten, D., Wöhling, T., Haslauer, C., Merchán, D., Causapé, J., Cirpka, O., 2014. Efficient calibration of a distributed pde-based hydrological model using grid coarsening. J. Hydrol. 519, 3290–3304.
Vargas-Amelin, E., Pindado, P., 2014. The challenge of climate change in Spain: Water resources, agriculture and land. J. Hydrol. 518, 243–249.
Whitehead, P.G., Wilby, R., Battarbee, R., Kernan, M., Wade, A., 2009. A review of the potential impacts of climate change on surface water quality. Hydrol. Sci. 54, 101–123.
Wilby, R., Wigley, T., 1997. Downscaling general circulation model output: a review of methods and limitations. Prog. Phys. Geogr. 21, 530–548.
Woznicki, S., Nejadhashemi, A., Parsinejad, M., 2015. Climate change and irrigation demand: uncertainty and adaptation. J. Hydrol. Reg. Stud. 3, 247–264.
Yokohata, T., Emori, S., Nozawa, T., Tsushima, Y., Ogura, T., Kimoto, M., 2005. Climate response to volcanic forcing: validation of climate sensitivity of a coupled atmosphere-ocean general circulation model. Geophys. Res. Lett. 32, L21710.
Zambrano-Bigiarini, M., Majone, B., Bellin, A., Bovolo, C.I., Blenkinsop, S., Fowler, H., 2010. Hydrological impact of climate change on the Ebro river basin. In: The Ebro River Basin. Springer-Verlag.
Zhao, F., Xu, Z., Zhang, L., Zuo, D., 2009. Streamflow response to climate variability and human activities in the upper catchment of the Yellow River Basin. Sci. China Ser. E: Technol. Sci. 52, 3249–3256.
Zheng, H., Zhang, L., Zhu, R., Liu, C., Sato, Y., Fukushima, Y., 2009. Responses of streamflow to climate and land surface change in the headwaters of the Yellow River Basin. Water Resour. Res. 45, W00A19.